Ultrashort-Pulse Phenomena

C. L. Tang
Cornell University, School of Electrical Engineering, Ithaca New York U.S.A.
D. E. Spence
Cornell University, School of Electrical Engineering, Ithaca New York U.S.A.

1. INTRODUCTION

There has been rapid progress in the generation of "ultrashort" optical pulses in recent years. In fact, the meaning of "ultrashort" in this context has been changing steadily over the years as shorter and shorter pulses are generated. It now generally means the subpicosecond down to the 5-fs range (Baltuska *et al.*, [1997]; Fork *et al.*, [1987]). Not only can optical pulses this short now be generated routinely; measurement techniques to characterize such pulses and schemes to use such pulses to study a variety of ultrafast physical and chemical processes and phenomena have also been developed. These advances followed from the invention of the laser and the technique of laser mode locking (see, for example, Smith *et al.*, [1974], or New, [1983]).

Mode locking causes thousands to many thousands of spectral components (the laser-cavity longitudinal modes) in the output of a suitably designed laser to be equally spaced in frequency and to have the same phase (Tang, [1990]). The width of these pulses is approximately equal to the inverse of the total spectral width of the laser output or the total number of spectral components times the spacing between the components. For a fully mode-locked laser with a total spectral width of several hundred angstroms in the visible or near infrared, for example, the corresponding pulse width would be down to the range of a few femtoseconds.

In practice, pulses down to tens of femtoseconds can now be generated fairly easily and used in various applications. Some of the earliest applications are in the study of relaxation dynamics of molecules and semiconductors and of material structures such as quantum wells in the subpicosecond time domain. In the case of bulk and quantum-well semiconductors, the interest is often in the relaxation mechanisms and the corresponding lifetimes of excited carriers in the conduction and valence bands. These are usually in the subpicosecond time domain and could previously be studied only indirectly. With the improved time resolution made possible by recent advances in the ultrafast optical sources and measurement techniques, these processes can now be studied and the corresponding lifetimes measured more directly. Relaxation dynamics down to the femtosecond time domain of excited vibronic states of molecules in all kinds of environments can be studied similarly and have attracted a great deal of attention.

In this article, we review the basic considerations in the generation, characterization, and some applications of ultrashort optical pulses. There is now a vast literature on the subject; only a few simple examples are reviewed briefly for tutorial purposes in the limited space available.

2. ULTRASHORT-PULSE PROPAGATION

The shape of a short intense optical pulse propagating in an unbounded medium can become distorted by the interplay between group-velocity dispersion (GVD) and light-induced index-of-refraction change in the medium (Shen, [1984]; Boyd, [1992]). These effects play an important role in the generation and propagation of ultrashort pulses (Martinez *et al.*, [1984]).

Consider a pulse with a slowly varying amplitude $A(z,t)$ of the form

$$E(z,t) = A(z,t)e^{i(k_0 z - \omega_0 t)} + \text{c.c.} \tag{1}$$

propagating through a medium with an intensity-dependent index of refraction of the form

$$n(z,t) = n_0 + n_2 I(z,t), \tag{2}$$

where $I(z, t) = (n_0 c/2\pi)|A(z, t)|^2$ is the intensity of the wave. Changing the time coordinate t to a retarded time $\tau?t - z/v_g$, where v_g is the group velocity of the pulse, it can be shown that the envelope function $A(z,t)$ satisfies a type of nonlinear Schrödinger's equation (Boyd, [1992]):

$$\frac{\partial A(z,\tau)}{\partial z} + \tfrac{1}{2}ik_2\frac{\partial^2 A(z,\tau)}{\partial \tau^2} = i\gamma|A(z,\tau)|^2 A(z,\tau), \tag{3}$$

where

$$k_2 = \left(-\frac{1}{v_g^2}\frac{\partial v_g}{\partial \omega}\right)_{\omega=\omega_0} \tag{4}$$

and v_g is the group velocity. k_2 describes the group-velocity dispersion, and

$$\gamma = n_2 n_0 \omega_0 / 2\pi \tag{5}$$

is the parameter responsible for self-phase modulation (SPM) in the medium. It is clear from Eq. (3) that if there is no GVD ($k_2 = 0$) and light-induced index-of-refraction change ($n_2 = 0$) in the medium, a pulse will propagate without distortion in the medium. Otherwise, a pulse of arbitrary shape will be distorted as it propagates in the medium because of the presence of GVD and SPM.

When there is GVD and SPM in the medium, it is possible under special conditions for the two effects to compensate each other, allowing a pulse to propagate in the medium undistorted. Such a situation can occur in the anomalous-dispersion regime if the pulse peak power exceeds a certain threshold value. The resulting special pulse is called a soliton (Bullogh and Candney, [1980]) and has the form

$$A(z,\tau) = A_0 \,\text{sech}(\tau/\tau_0)e^{i\kappa z}, \tag{6}$$

where the pulse peak amplitude A_0, phase shift κ, and width τ_0 are related:

$$|A_0|^2 = -k_2/\gamma\tau_0^2, \tag{7}$$

$$\kappa = -k_2/2\tau_0^2. \tag{8}$$

It can be shown that a solution of the form (6), subject to the special conditions (7) and (8), indeed satisfies Eq. (3). Substituting (6) into (1) gives a pulse envelope that is only a function of the retarded time τ, which represents a pulse propagating in the medium undistorted at the group velocity v_g. Soliton-like formation is one mechanism involved in the generation of ultrashort pulses in lasers (Martinez *et al.*, [1984]), and solitons propagating in low-loss fibers may possibly have important applications in future high–data-rate long-distance telecommunication systems (Agrawal, [1989]).

Pulse shaping on a femtosecond time scale has also been proposed and demonstrated by Weiner *et al.* ([1992]) using a multielement liquid-crystal modulator to manipulate the phases of spatially dispersed optical-frequency components and by Hillegas *et al.* ([1994]) using an acousto-optic modulator as a spatial modulator in a zero-dispersion line.

3. GENERATION OF ULTRASHORT PULSES

3.1. Basic Ultrafast Laser Sources

The use of laser mode-locking techniques to generate short optical pulses has a long history (Smith *et al.*, [1974]; New, [1983]; de-Maria *et al.*, [1966]). The pulse width that can be generated has steadily decreased from the picosecond range down to the 5-fs range (Baltuska *et al.*, [1997]). The basic concept of mode locking can best be explained in the frequency domain as follows.

A laser consisting of a gain medium with a frequency-dependent index of refraction $n(v)$, completely filling a Fabry–Pérot type of cavity of length L, can have many longitudinal modes with the frequency spacing $\Delta v = c/2n(v)L$, which is the reciprocal of the optical round-trip time in the cavity at the frequency v. As a result of dispersion within the cavity, the spacing between the resonance frequencies of the longitudinal modes changes with the mode frequency v. In general, the laser oscillates in many slightly unequally spaced longitudinal modes, and the phases of these modes are unrelated. If all the oscillating modes can be forced to be equally spaced at Δv_f and in phase at one instant of time, then the mode amplitude will add resulting in an intensity maximum. After a time $t = 1/N\Delta v_f$, the phases of the modes have changed by enough relative to each other so that the total field amplitude is zero. The result is a sequence of short mode-locked pulses separated by $1/\Delta v_f$. The width of the pulses will be approximately equal to the inverse of the total bandwidth of the laser output, or $1/N\Delta v_f$, where N is the total number of oscillating laser modes. Thus, for lasers with a large bandwidth (deMaria *et al.*, [1966]; Fork *et al.*, [1981]) such as dye lasers and Ti:sapphire lasers (Spence *et al.*, [1991]), the pulse widths can be very short indeed.

There are many different laser mode-locking techniques, but all have to provide two basic functions: forcing all the modes to be equally spaced and forcing them to have the same phase at one instant of time.

In the active mode-locking schemes, the gain in the laser medium or the loss of some intracavity element is externally modulated at a frequency Δv_f close to most of the cavity

mode spacings and, therefore, also matching the cavity round-trip frequency. Periodic amplitude modulation forces the oscillating laser modes to be equally spaced in the frequency domain. If this modulation is large enough, it can also overcome the forces that make the phases of oscillating modes to be randomized and thus forces the modes to add coherently in time. In the time domain, amplitude modulation at a rate corresponding to the cavity round-trip time favors the formation of a single pulse in the cavity that passes through the modulator at the instant when its transmission is a maximum.

In passive mode-locking lasers, there is usually a nonlinear element in the cavity that leads to less loss, or higher gain, at higher intracavity laser intensity. Thus, as the laser intensity builds up from random noise spikes, the highest-intensity spike will be favored at the expense of the other spikes. Under favorable conditions, this spike will in time become the only surviving short pulse circulating in the laser cavity. This is equivalent to forcing the laser modes to be equally spaced in frequency and add coherently at the peak of the pulse. The laser output will consist of a train of repetitive short pulses due to periodic incidence of this circulating pulse on the output mirror of the laser.

3.1.1. Mode-Locked Rhodamine 6 G Dye Lasers

Commonly used ultrashort laser sources tend to be passively mode locked, because it is more efficient and, hence, of more practical importance. Until recently, the most widely used ultrashort laser sources were of the type derived from one form or another of rhodamine 6 G (Rh6 G) dye laser with an intracavity saturable absorber such as DODCI oscillating at 630 nm (Fork *et al.*, [1981]). These have recently largely been superseded by mode-locked solid-state Ti:sapphire lasers (Spence *et al.*, [1991]).

3.1.2. Mode-Locked Ti:Sapphire Lasers

Solitonlike pulse propagation plays a major role in ultrashort-pulse formation in the Ti:sapphire laser (Haus *et al.*, [1992]; Krausz *et al.*, [1992]; Chilla and Martinez, [1993]). Because of the small beam size (~50 μm) in the relatively long (~20 mm) gain medium, the effects of GVD and SPM are significant. Further, for femtosecond-pulse generation, a two-prism sequence is usually inserted into the cavity to provide negative (anomalous) GVD. Thus, all the elements for soliton formation are present. There is, however, one important difference between mode-locked pulses in these lasers and in optical fibers. In the laser, the negative GVD and SPM act at different discrete locations in the cavity, but in optical fibers, these effects act continuously along the length of the fiber. The result is that the mode-locked pulses in the laser are not stable and tend to break up in the wings. In order for stable mode-locked pulses to exist, there needs to be a passive saturable absorber that can suppress the pulse breakup. This fast saturable absorption is provided through the light-intensity–induced focusing effect due to the nonlinear Kerr effect (Salin *et al.*, [1991]) [light-induced index-of-refraction change that is proportional to the intensity of the light; see Eq. (2)] in the Ti:sapphire crystal. A strategically located aperture in the cavity can present less loss to a high-intensity light pulse than to a continuous light wave (Spinelli *et al.*, [1991]), thus acting as saturable absorber. This differential loss can force the laser to operate in the mode where a single pulse circulates in the cavity and produces mode locking. Because the gain bandwidth of Ti-sapphire can be very wide—hundreds of angstroms—ultrashort pulses down to a few femtoseconds can potentially be generated in such a laser. Alternatively, such a laser can be

tuned from almost 700 nm to 1 μm and the average power, cw or mode-locked, can be in the 2–3-W range as compared to at most a few hundred milliwatts typical of a mode-locked Rh6 G dye laser. The solid-state Ti:sapphire laser along with various wavelength-conversion devices have, thus, largely replaced the dye laser in most applications.

While the mode-locking process can be described qualitatively relatively easily on the basis of the above frequency-domain picture, it is not possible to develop any quantitative theory of the laser on the same basis. For in a typical femtosecond laser, there can be more than a hundred thousand simultaneously oscillating modes. The problem of nonlinear interaction of such a large number of modes is obviously extremely complex.

Most attempts at quantitative analysis of the femtosecond laser follow the time-domain picture based on a master equation in the time domain describing gain, loss, phase shift, dispersion, and nonlinearity (Haus *et al.*, [1991, 1992]; Krausz *et al.*, [1992]). A truly successful comprehensive quantitative theory for ultrashort lasers has yet to be developed. Even in the absence of such a theory, the development of ultrashort lasers has been very rapid. Commercial mode-locked dye and Ti:sapphire lasers are now widely available.

Given a basic ultrafast laser source with the power and wavelength ranges typically available from a dye or Ti:sapphire laser, there are various schemes to increase the energy per pulse and to extend the wavelength range. The available energy per pulse can be increased dramatically by using power amplifiers of one form or another. Such a gain is usually achieved at the expense of pulse repetition rate leaving the average power typically still in the range of less than 1 W.

3.1.3. Mode-Locked Fiber Lasers

Since the first single-mode rare-earth–doped optical fiber was pulled in 1973 (Stone and Burrus, [1973]), there has been significant effort invested in the development of mode-locked fiber lasers. These are particularly attractive because of their wide bandwidth and high gain. In addition, they are robust, compact, solid-state sources, with the potential for easy integration into optical-fiber communications systems. The ideal mode-locked fiber laser is an all-fiber device pumped by a diode laser and capable of emitting pulses having durations less than half a picosecond.

Fiber lasers differ from other solid-state lasers in a number of ways. Most importantly, the fiber laser has a much higher gain (up to 10^4), allowing relatively lossy optical components to be integrated into its cavity; it also has strong mode confinement so that nonlinear effects are likely to be significant. (As we have already mentioned, it is these effects that ultimately determine the pulse duration.) Consequently, the erbium-doped (Er) fiber laser has attracted the most interest because it operates at a wavelength of ~1.5 μm, which is at a low-loss window of passive optical fibers, and is also longer than the zero-dispersion wavelength, so that soliton pulse formation can be exploited.

Several mode-locking schemes for fiber lasers have emerged over the years, including saturable absorbers (Dzhibladze *et al.*, 1993), amplitude (Duling *et al.*, [1988]) and phase modulators (Geister and Ulrich, [1988]), nonlinear mirrors (Hofer *et al.*, [1992]), and nonlinear pulse compressors (Hofer *et al.*, [1990]). An actively mode-locked Er-fiber laser has generated pulses as short as 2.8 ps (Kafka *et al.*, [1989]; Smith *et al.*, [1991]). Not

surprisingly, the shortest pulses have been generated from passively mode-locked fiber lasers. The first of these used a nonlinear optical loop mirror (NOLM) and could generate pulses as short as ~200 ps (Doran and Wood, [1988]). A variant of this laser, the nonlinear amplifying loop mirror (NALM), has an amplifier included in the loop mirror section (Duling, [1991]; Richardson *et al.*, [1991]).

One problem with this laser is due to the fact that the pulses propagate as solitons that have quantized energy (Grudinin *et al.*, [1992]). This can lead to undesirable effects including multiple pulsing, an unstable repetition rate, and dispersive wave shedding, as the pulses adjust their peak power to that of the soliton. A solution to this problem is the stretched-pulse mode-locked fiber ring laser. This laser has segments of large positive- and negative-dispersion fiber in the cavity. The pulse width can change by an order of magnitude as it propagates within the cavity, thus lowering the peak power compared to that of an unchanging pulse. The chirp of the resulting output pulse is highly linear and can be efficiently compensated for by using an appropriate length of output coupling fiber. Sub-100-fs pulses have been generated from such an all-fiber laser (Tamura *et al.*, [1993]).

With the increased understanding of the principles involved in the operation of the mode-locked fiber laser, these devices have already become a practical (almost ideal) source of ultrashort pulses, rather than just another perpetual technology of the future.

3.1.4. Mode-Locked Semiconductor Lasers

Because of the wide range of potential applications of ultrafast semiconductor sources, in electronics in particular, there has been a great deal of interest in mode-locked semiconductor lasers. The problem is, however, a difficult one for several reasons. Because the cavity length of usual solitary semiconductor lasers is typically no more than a few hundred microns, the mode spacings are relatively large and highly unequal on account of the material dispersion in the semiconductor gain medium. It is generally only possible to lock a few modes leading to a relatively small temporal finesse (defined by the pulse repetition time divided by the pulse width), typically less than 10. When the finesse number is small, the pulse peak is less precisely determined on a time scale corresponding to the pulse repetition time. For many applications, a finesse number of 10 is too small of practical use. Most potentially useful mode-locked semiconductor lasers involve, therefore, the use of external cavities. The pulse widths and quality of such lasers are generally poor, however, because it is extremely difficult to eliminate completely the mode structure due to the semiconductor laser diode chip itself.

3.2. Frequency-Conversion Devices

In the last few years, there have been significant advances in extending the wavelength range of ultrafast sources through nonlinear frequency-conversion schemes. These include harmonic, sum- and difference-frequency, and parametric processes. Through these schemes, femtosecond sources from 315 nm to almost 20 μm are now available. These frequency-conversion processes preserve the basic characteristics of the pulse with the exception of power. For intracavity conversion, the conversion efficiency can be relatively high, up to the ~50% range. For extracavity conversion, the efficiency is generally lower depending upon the nonlinear crystal used and the pulse characteristics.

The wavelength of the Rh6 G dye-laser output can be extended to around the 300–340-nm range through frequency doubling, either directly (Edelstein *et al.*, [1988]) or after amplification. BBO (beta-barium borate) crystals are typically used for this purpose. The GVD of this crystal for second-harmonic generation at 640 nm is approximately 360 fs/mm. Thus, to avoid pulse broadening, the doubling crystal must be very thin. With a polished thin BBO crystal of ~50 μm for frequency doubling, the dye-laser output pulse characteristics can basically be preserved down to the range of a few femtoseconds. For intracavity doubling (Ellingson and Tang, [1992]), the effective conversion efficiency can be nearly 100% even for such thin crystals, if the doubling process represents the only loss process to the laser at the fundamental frequency.

For the visible region, doubling of the Ti:sapphire laser can provide tunable femtosecond pulses in the 350–550-nm range (Ellingson and Tang, [1992]). Again, with intracavity doubling using thin BBO crystals, relatively high average power (to 230 mW) and high conversion efficiency (to ~75%) have been achieved.

Difference-frequency generation by mixing two laser outputs at two different frequencies in various nonlinear optical crystals can extend the basic tuning range of such primary femtosecond sources as Rh6 G dye lasers and Ti:sapphire lasers into the near- and mid-infrared. However, the conversion efficiency tends to be low especially in the case where the mixing takes place external to the laser cavity. Furthermore, in the ultrashort-pulse domain, synchronizing two independent femtosecond sources presents special technical problems (Spence *et al.*, [1993]).

A more powerful and versatile technique uses parametric conversion (Edelstein *et al.*, [1989]; Tang and Cheng, [1996]; Zhang *et al.*, [1996]). Efficient and powerful femtosecond optical parametric sources are now available for most of the near- to mid-infrared range to about 5.2 μm (Spence *et al.*, [1996]). With suitable crystals, the wavelength range can potentially be extended to the 20-μm range (Tang and Cheng, [1996]).

In the parametric process (Tang and Cheng, [1996]; Zhang *et al.*, [1996]), a photon at frequency ω_p propagating in a nonlinear medium is converted into two lower-frequency photons at ω_1 and ω_2 where the photon energy and momentum conservation conditions are satisfied:

$$\hbar\omega_p = \hbar\omega_1 + \hbar\omega_2, \tag{9}$$

$$\hbar k_p = \hbar k_1 + \hbar k_2, \tag{10}$$

taking into account the dispersion relation $k = n(\omega)\omega/c$.

The energy conservation condition, (9), is automatically satisfied. Special arrangement is required, however, to satisfy the momentum conservation condition, (10), which is also called the phase-matching condition. There are two types of phase-matching conditions, type I and type II. In anisotropic uniaxial crystals, for example, the magnitude of the wave vector for the extraordinary waves is a function of the propagation direction of the wave, θ_p, relative to the crystal axis. More specifically, for a negative uniaxial crystal, for example, under the so-called type-I phase-matching condition, the extraordinary pump wave and the ordinary ω_1 and ω_2 waves are orthogonally polarized, and the corresponding phase-matching condition is

$$\hbar k_p^{(e)} = \hbar k_1^{(0)} + \hbar k_2^{(0)}, \tag{11}$$

where

$$k_p^{(e)}(\omega_p, \theta_p) = n^{(e)}(\omega_p, \theta_p)\omega_p/c, \tag{12}$$

$$k_{1,2}^{(0)}(\omega_{1,2}) = n^{(0)}(\omega_{1,2})\omega_{1,2}/c. \tag{13}$$

Each pair of specific frequencies, ω_1 and ω_2, implies a particular phase-matching angle θ_p for a particular pump-wave frequency ω_p. Solving Eqs. (9)' (12), and (13) gives the phase-matching equation

$$\frac{\cos^2(\theta_p)}{n_p^{(e)^2}} + \frac{\sin^2(\theta_p)}{n_p^{(0)^2}} = \frac{\omega_p^2}{[n_1^{(0)}\omega_1 + n_2^{(0)}\omega_2]^2}, \tag{14}$$

which gives the phase-matching angle for each set of frequencies. Therefore, ω_1 and ω_2 can be tuned by rotating the crystal angle, θ_p, relative to the pump-beam direction. For type II phase matching, the generated waves at ω_1 and ω_2 are also orthogonally polarized (i.e., one is an extraordinary wave as the pump wave and the other is an ordinary wave).

In the spontaneous parametric process, an ω_p photon spontaneously breaks down into an ω_1 photon and an ω_2 photon. In the stimulated process, ω_1 photons and ω_2 photons are amplified, as in a repeated difference-frequency generation, at the expense of ω_p photons. The optical parametric process is a single three-photon process; the spatial and temporal coherence properties of the generated waves at ω_1 and ω_2 are directly related to those of the pump wave. An ultrashort pump pulse will generally lead to ultrashort pulses at the generated frequencies ω_1 and ω_2 as modified by such effects as GVD and SPM discussed in Sec. 3.

The useful input of an optical parametric amplifier is either the spontaneous parametric emission or output of another optical parametric oscillator at a lower output level. In an optical parametric oscillator, the only input beam is the pump beam at ω_p. The oscillator output is initiated by the spontaneously emitted photons at ω_1 and ω_2 followed by amplification through the stimulated parametric process. With the addition of a suitable form of optical feedback, such as a Fabry–Pérot cavity as in a laser, the amplified noise can grow and continue to convert and deplete the pump beam until the parametric gain is saturated at the level equal to the cavity loss. With high enough pump power and low enough cavity loss, the corresponding conversion efficiency of the oscillator can be very high, often reaching 30–60% of the incident pump power.

A great variety of femtosecond optical parametric oscillators have been reported in recent years. The pump sources are generally either mode-locked Rh6 G dye lasers or mode-locked Ti:sapphire lasers. The most commonly used nonlinear crystals are the KTP ($KTiPO_4$) isomorphs [see Fig. 1 for examples of the wide tuning range covered by the femtosecond optical parametric oscillators (OPO) using these crystals], $LiNbO_3$, or $KNbO_3$. Generally speaking, pulse widths down to 50 fs and average power in the hundreds of milliwatts range at 10^8-Hz repetition rate are now available in the 1- to 5-μm range. With crystals such as

$AgGaS_2$ or $AgGaSe_2$, the tuning range can potentially be extended to the 20-µm range, once suitable pump sources become available in the 1–1.5-µm range.

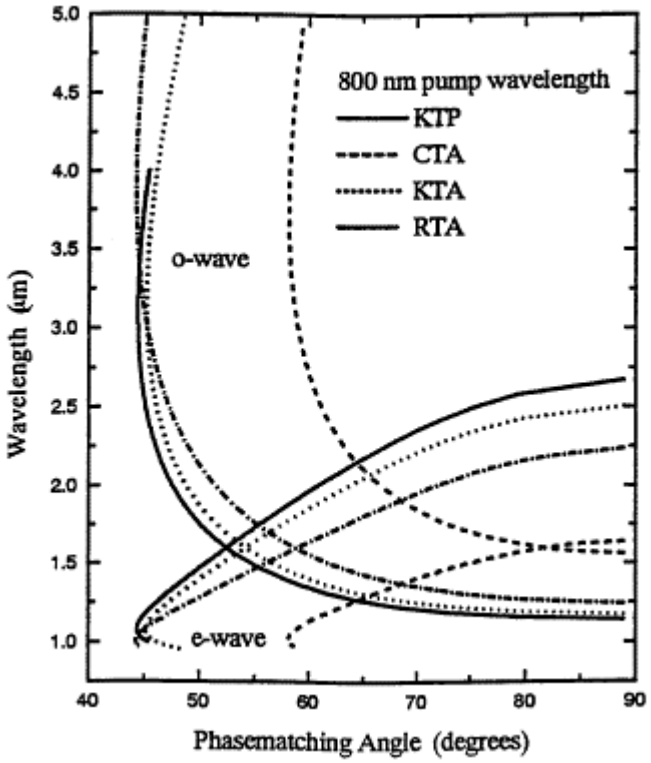

Figure 1 Calculated tuning curves for the OPO's based on the materials KTP ($KTiOPO_4$), KTA ($KTiOAsO_4$), CTA ($CsTiOPO_4$), and RTA ($RbTiOPO_4$).

To extend the tuning range to the shorter wavelengths, it is again possible to use nonlinear optical conversion processes such as intracavity or extracavity second-harmonic generation or sum- or difference-frequency processes. Some of these schemes have already been demonstrated. For example, through intracavity doubling in BBO, the output of a KTP femtosecond OPO can be extended to the spectral range from 580 nm to 1.1 µm at an average power level on the order of 200 mW.

In addition to parametric oscillators, a variety of optical parametric amplifiers (OPAs) have been demonstrated and used in a variety of experiments. Commercially available OPAs range from mJ/pulse at 10^5 Hz to tens of mJ/pulse at lower repetition rates.

In conclusion, femtosecond optical parametric oscillators and amplifiers using a variety of nonlinear optical crystals and pump lasers are effective sources of broadly tunable ultrashort radiation.

4. FEMTOSECOND MEASUREMENT TECHNIQUES

4.1. Measurement and Characterization of Ultrashort Pulses

To characterize such short pulses, conventional photodetectors do not have fast enough response times. Special measurement techniques are needed. For example, instead of direct

time-domain measurements, the general practice is to determine the pulse duration by measuring the spatial extent of the pulse through some kind of second-order intensity-autocorrelation measurement using an interferometric arrangement such as that shown in Fig. 2. In such a measurement, the pulse is first split into two. One of the pulses is delayed from the other with a variable delay τ. The two pulses are then sent into a thin nonlinear crystal. When the delay τ is such that the two pulses overlap in the crystal, the second harmonic has a higher intensity than when the pulses do not overlap. The second-harmonic intensity as a function of τ gives the intensity autocorrelation trace of the pulse. If the pulse shape is known, the width of the pulse can be determined from its intensity autocorrelation trace (Sala *et al.*, [1980]). In this way, the problem of measuring a temporal event of the order of $\leq 10^{-12}$ s is transformed into the relatively simple task of measuring the spatial extent of an autocorrelation function of ~0.3 mm.

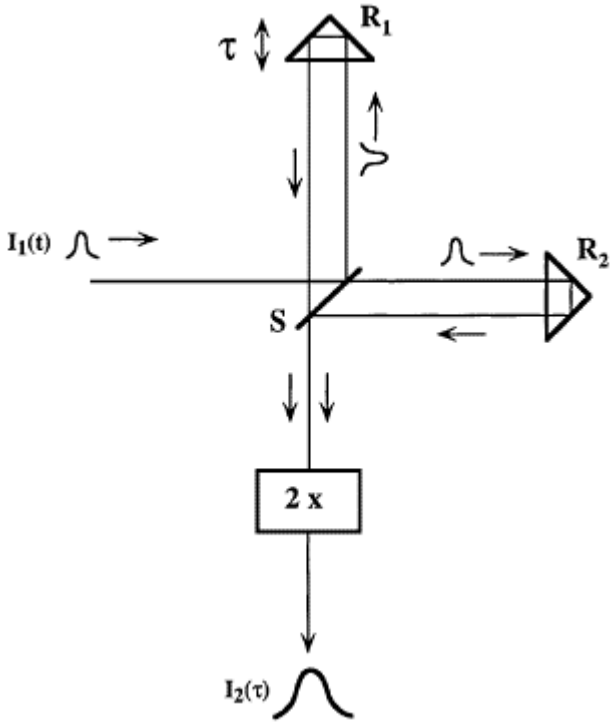

Figure 2 Intensity autocorrelation measurement setup. S = beam splitter; $R_{1,2}$ = retroreflectors.

With an interferometer type of arrangement with a suitable nonlinear optical crystal in one of the arms as shown in Fig. 2, the background-free part of the second-order intensity autocorrelation

$$\mathrm{AC}(\tau) \equiv \frac{\int_{-\infty}^{\infty} I(t)I(t-\tau)dt}{\int_{-\infty}^{\infty} I(t)I(t)dt} \tag{15}$$

can be measured. The relationship between the width of the pulse and the width of AC(τ) depends upon the pulse shape. For the commonly assumed hyperbolic-secant pulses, the ratio of the pulse width to the autocorrelation width is 0.65 and the product of the pulse width and bandwidth pulse is $\Delta\nu\Delta\tau \approx 0.315$ for ideal transform-limited pulses. For Gaussian pulses, the corresponding numbers are 0.71 and 0.44, respectively. The corresponding numbers for the

other pulse shapes are tabulated by Sala *et al.* ([1980]) and Weiner ([1983]). The pulses can also be similarly characterized by measuring the cross-correlation with other pulses of known shapes through the sum- or difference-frequency processes.

For an ideal transform-limited pulse, the interferometric autocorrelation trace will also give information on the pulse width and should have a peak-to-background ratio of 8:1. A typical trace is shown in Fig. 3. If the pulse is frequency chirped by group-velocity dispersion, or self-phase modulation, or whatever the reason, then there will be a loss of coherence in the wings of the interferometric autocorrelation trace, thus giving a false reading of the pulse width.

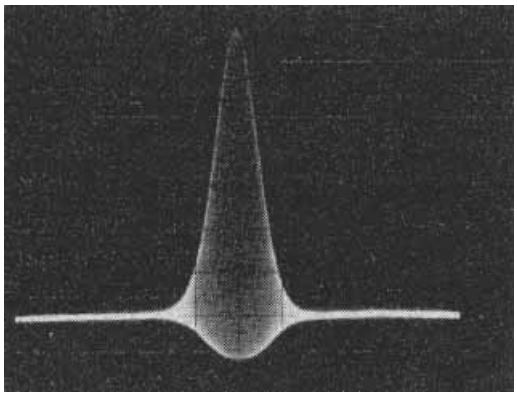

Figure 3 Example of interferometric autocorrelation trace.

4.2. Frequency-Resolved Optical-Gating (FROG) Technique

When there is chirping in the pulse, the problem of accurately characterizing the amplitude and phase of a femtosecond pulse is a difficult one. One technique (Kane and Trebino, [1993]; Trebino and Kane, [1993]) is to use frequency-resolved optical gating or FROG. In this technique, a signal $E_{\text{signal}}(t, \tau)$ is generated in an instantaneously responding optical Kerr medium that is the product of the pulse field to be measured, $E(t)$, and the intensity profile of a delayed replica of the same pulse:

$$E_{\text{signal}}(t,\tau) \alpha E(t)|E(t-\tau)|^2. \tag{16}$$

A spectrum of $E_{\text{signal}}(t, \tau)$, called FROG trace, is then recorded:

$$I_{\text{FROG}}(\omega,\tau) \alpha \left| \int_{-\infty}^{\infty} E_{\text{signal}}(t,\tau) \exp(-i\omega t) dt \right|^2. \tag{17}$$

The FROG trace can be inverted to yield the amplitude and phase of the original pulse field $E(t)$ by a numerical procedure that has been proposed by Kane and Trebino ([1993]).

4.3. Pump-and-Probe Measurement Techniques

"Pump and probe" is a commonly used generic type of technique for studying ultrafast processes in various materials and structures (Ippen and Shank, [1977]; Goebel, [1992]). In

such measurements, the population of an initial state in the material or structure is first perturbed with a short pump pulse. The relaxation dynamics of the same initial state of the perturbed system, or other states to which the excited initial population has relaxed, is then measured by probing at successively delayed time intervals.

Figure 4 shows a schematic diagram of a typical pump-and-probe measurement setup. The basic operation of the setup is similar to the autocorrelation measurement scheme shown in Fig. 2. The main difference is that the nonlinear crystal in the latter is replaced in the former by the sample to be measured. Again, the input pulse is first split by the beam splitter *S* into two. The two pulses are then directed into the sample, crossing the same region of the sample at a small angle and with one of the pulses delayed by a variable delay τ relative to the other. The first pulse acts as a pump that perturbs the sample, and the second pulse probes the state of an illuminated region of the sample at the time τ. The detector measures the power of the transmitted probe pulse as a function of the delay time τ. The practical implementation of the pump-and-probe measurement technique will obviously depend upon the actual material being studied. Consider for example an atomic or molecular system as shown schematically in Fig. 5(a). Suppose all the atoms or molecules are initially in the ground state (1). An incident short pump pulse creates a population increase Δn_2 in the excited state (2) with a corresponding population decrease $-\Delta n_1$ in the ground state. To the lowest order, both Δn_1 and Δn_2 are proportional to the pump pulse intensity I_{pump}. Through various relaxation processes, these perturbed populations will change with time. In the commonly used form of pump–probe technique, the transmission of a probe pulse through the sample at a delay time τ is measured, which depends on $\Delta n_2(\tau)$ and $\Delta n_1(\tau)$. It often happens that the excited-state population relaxes to some intermediate state (3) quickly, but the ground-state population does not recover within the scanning range of the probe pulse delay, leaving $\Delta n_1(\tau)$ essentially at its initial value $\Delta n_1(0)$ during the measurement. The corresponding transmitted probe intensity, $P(\tau)$, typically has the form shown in Fig. 5(b). Qualitatively, the decay part of the probe intensity is a measure of $\Delta n_2(\tau)$, which describes the relaxation dynamics of the excited state. The step that persists after the initial decay corresponds to $\Delta n_1(\tau) \approx \Delta n_1(0)$.

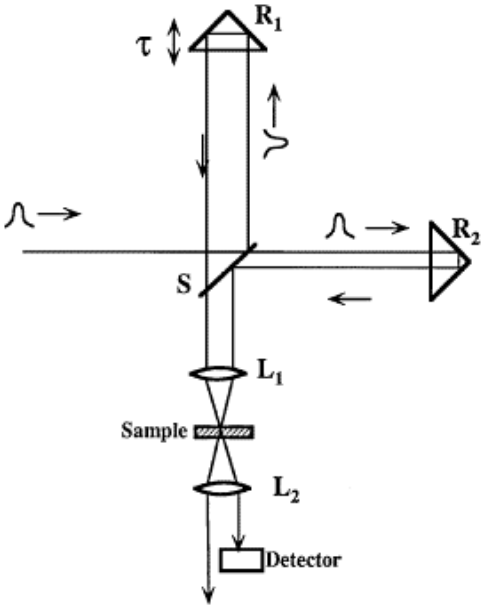

Figure 4 Pump–probe measurement setup. S = beam splitter; $R_{1,2}$ = retroreflectors; $L_{1,2}$ = lenses.

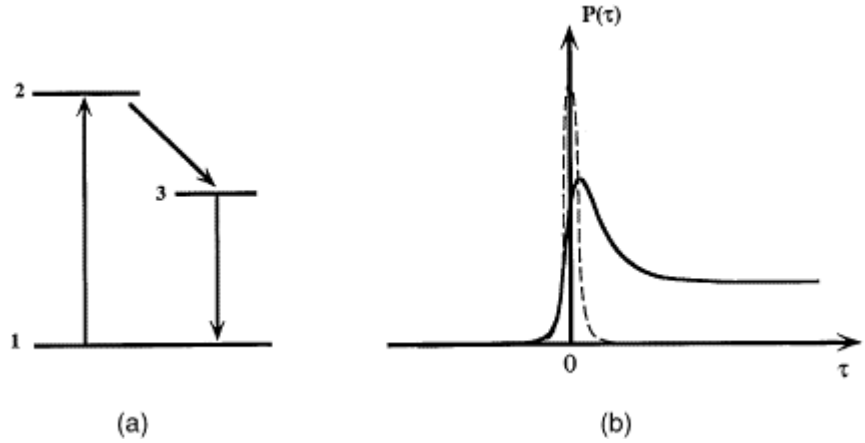

Figure 5 (a) Schematic of atomic- or molecular-level scheme in pump–probe measurements. (b) Pump–probe trace (solid line) and autocorrelation trace of pump or probe pulse (dashed line).

In the cases where the excited-state relaxation process can be represented by a single exponential process and the corresponding relaxation time T_0 is long compared with the pulse width but much shorter than the ground-state recovery time, it is relatively straightforward to obtain an estimate of T_0 from the measured decay part of the probe-intensity trace of the form shown in Fig. 5(b) by curve fitting outside the pulse-overlap region. Within the pulse-overlap region, there is a so-called coherent-artifact (Ippen and Shank, [1977]) contribution, which is an extra signal that does not depend upon the relaxation dynamics of the population change in the sample and must be excluded from the curve fitting.

For those cases where the above conditions do not hold, there are generally several points to be considered in the quantitative analysis of the data. First, when the relaxation times approach the pulse width, the finite widths of the pump and probe pulses make it difficult to pinpoint the $\tau = 0$ point in a pump–probe data trace. Second, it is difficult to delineate and exclude the effects of the coherent artifact in the pulse-overlap region from the data analysis. Third, when the relaxation dynamics are complicated and more than one or two exponential, or nonexponential, processes are involved, to extract multiple relaxation times from a single measured decay curve requires sophisticated analysis and highly accurate data, which often necessitates signal averaging at high pulse repetition rates. Fourth, the presence of any relaxation process that is much slower than the processes being measured complicates the data analysis and leads to ambiguity in determining the baseline for analyzing the fast processes. Experimentally, it also means that the pulse repetition time or the recycling time must be long compared with the slow relaxation time. A lower pulse repetition rate leads to longer averaging time. Some of these problems can be alleviated with the optical-correlation spectroscopic technique as is discussed in Sec. 4.4.

4.4. Optical-Correlation Spectroscopy

Optical-correlation spectroscopy, or two-pulse correlation spectroscopy (Taylor *et al.*, [1985]), is a symmetrized version of the pump–probe technique discussed in Sec. 4.2. A

schematic of the setup is shown in Fig. 6. The only difference between this scheme and that shown in Fig. 4 is that, in the symmetrized version, the total transmission of both pulses, not just the probe pulse, through the sample as a function of the variable delay (τ) between the two is measured. For positive τ, one of the pulses is the pump and the other is the probe; for negative τ, the role of the pulses is reversed. To the lowest order in absorption saturation, which is proportional to the square of the total incident intensity, the effect of each pulse on the other is the same for the same magnitude of τ; the measured total transmission is, therefore, a symmetric function of τ. The signal typically has a peak near $\tau = 0$, called TCP (transmission-correlation peak), as shown schematically in Fig. 7. The TCP is a symmetrized version of the pump–probe signal in the following sense:

$$\mathrm{TCP}(\tau) \propto [P(\tau) + P(-\tau)]. \tag{18}$$

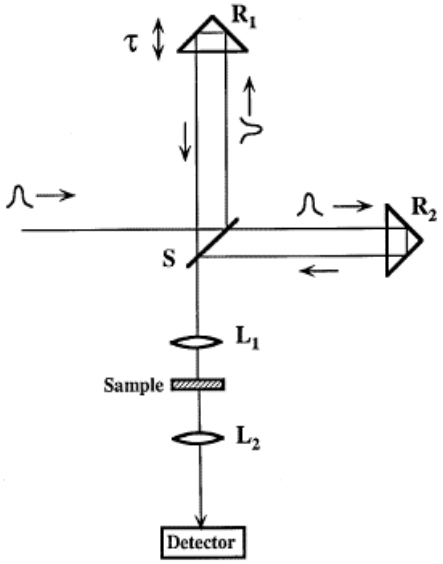

Figure 6 Transmission-correlation measurement setup. S = beam splitter; $R_{1,2}$ = retroreflectors; $L_{1,2}$ = lenses.

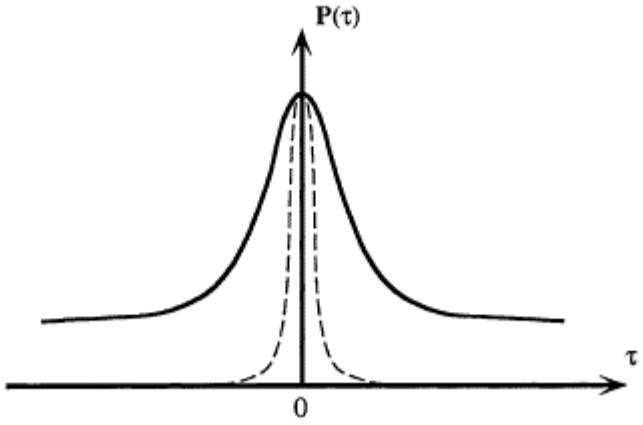

Figure 7 Transmission-correlation peak (solid line) and autocorrelation trace of pump and probe pulses (dashed line).

Optical-correlation spectroscopy resolves (Taylor *et al.*, [1985]) some of the difficulties associated with the conventional pump–probe spectroscopy described above (Sec. 4.3): First, because of the symmetry, the zero delay point $\tau = 0$ is unambiguously determined without the need for any additional experiments. Second, the slow process gives basically a constant background on the fast time scale and can, therefore, be automatically subtracted experimentally from the data on the fast time scale. Third, the symmetry in the TCP is a real-time indicator of proper alignment of the beams; this is an important experimental tool that is lacking in the conventional asymmetric pump–probe measurements. The difficulty associated with the coherent artifact within the pulse-overlap region remains, however; but it is no better or worse using either version of the pump–probe method.

Optical-correlation spectroscopy has also been widely used to study ultrafast processes in semiconductors and molecules.

5. ULTRAFAST PROCESSES IN MOLECULES AND SEMICONDUCTORS

With the increased time resolution made possible by the femtosecond lasers, many new ultrafast processes can be studied. Some of the earliest applications were in semiconductors and molecules.

5.1. Femtosecond Relaxation in Bulk Semiconductors and Quantum-Well Structures

In the case of semiconductors, a classic problem is to determine the intrinsic lifetime of Bloch states in the conduction band (Taylor *et al.*, [1985]; Tang *et al.*, [1988]). This problem is of particular interest for applications, as it is the lifetime that limits the ultimate speed of any electronic device that makes use of such a semiconductor. The arrangements typically used to measure this intrinsic lifetime are shown schematically in Figs. 4 and 6. Electrons are excited from the valence band into the conduction band by ultrashort pulses. Some of the relevant questions are: How long does an excited electron stay in the initial state and by what mechanisms does the electron relax from the initial state to the bottom of the conduction band? Once relaxed to the bottom of the conduction band, how long does it take the electron distribution to eventually cool to the lattice temperature? These different stages of relaxation process generally take place in from tens of femtoseconds to tens of picoseconds.

Consider, for example, GaAs. The corresponding band structure near the zone center is shown schematically in Fig. 8. The sample is typically in the form of a thin film (~200 nm) of epitaxially grown $Al_xGa_{1-x}As$. At 630 nm, corresponding to the Rh6 G dye-laser output, the excited electronic states from the heavy- and light-hole valence-band states are at approximately 0.5 eV above the band edge of the conduction band. The electrons excited from the split-off band are near the conduction-band edge. Because of the significant difference in the density of states, most (~80%) of the excited electrons are from the heavy- and light-hole states. With femtosecond pulse excitation, the holes generated in the valence band typically relax quickly. The saturation in the transmission through the sample of a suitably delayed probe pulse at the same wavelength as that of the pump pulse measures primarily the dynamics of the electron population in the initially excited conduction-band states. The measured transmission as a function of the probe pulse delay gives, therefore, the relaxation dynamics of the electrons from the initial state. Figure 9 shows a typical pump–

probe trace and a transmission-correlation trace for bulk GaAs at room temperature. Deconvolution of the pump–probe or the transmission-correlation trace outside the coherence peak region with the autocorrelation trace of the probe pulse followed by appropriate data reduction gives the corresponding time constants of the relaxation processes that contribute to the decay of the population from the initially excited states.

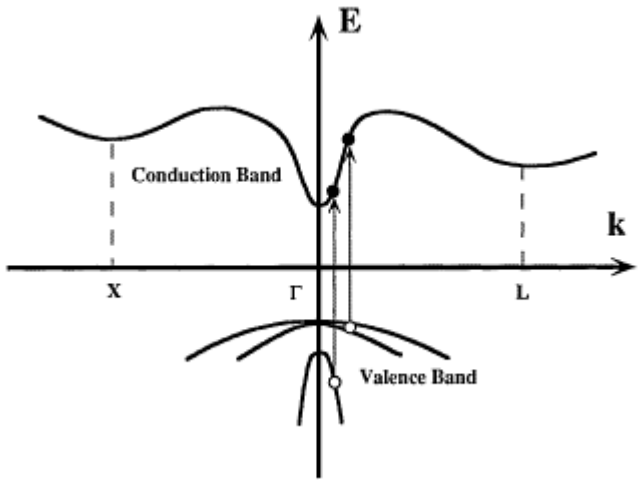

Figure 8 Excitation of electron and hole distributions in GaAs by Rh6 G dye-laser output at 630 nm.

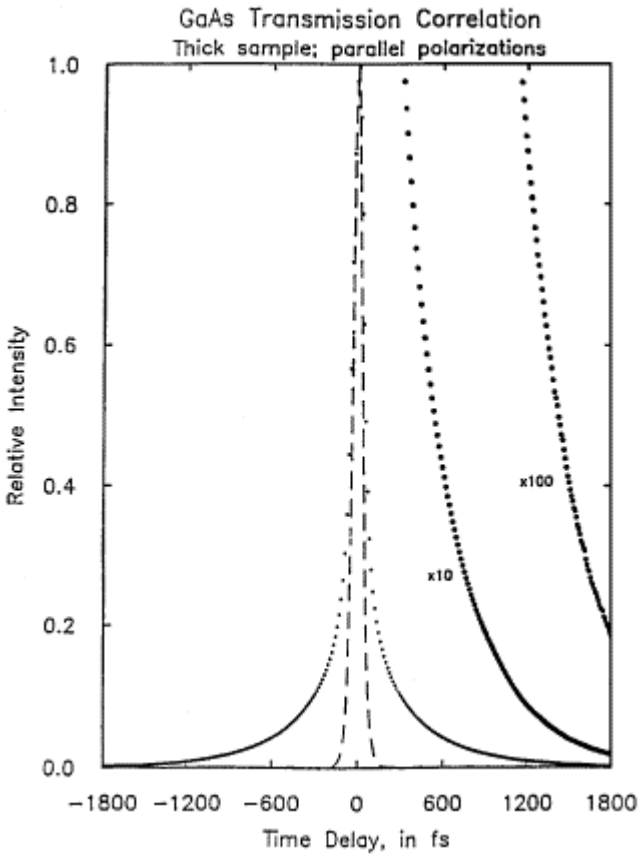

Figure 9 Example of transmission-correlation trace corresponding to hot-carrier relaxation at ~0.5 eV above the conduction-band edge of GaAs.

The nonequilibrium distribution in the conduction band typically relaxes in several stages and through different mechanisms depending on the carrier concentration. At low carrier concentrations ($<<10^{-16}$ cm^{-3}), carrier–carrier scattering is less important. In the absence of carrier–carrier scattering, the initial relaxation mechanism is due to optical phonon emission within the central valley, with a relaxation time on the order of 150 fs, and polar optical-phonon scattering into the excited states of the satellite valleys, with a time constant on the order of 40–50 fs. These carriers decay quickly to the bottom of the satellite valleys, from which they scatter in less than a picosecond back into the central valley at about 0.3 eV above the band edge. Once in the central valley, through optical-phonon emission, the electrons continue to decay to and thermalize near the bottom of the central valley in a few picoseconds. The corresponding electron temperature at this stage is, however, generally higher than the lattice temperature, and it takes tens of picoseconds for the temperature to equalize eventually.

Because of the possible presence of multiple relaxation processes, quantitative interpretation of the pump–probe or the transmission-correlation trace requires care. The procedure of linear prediction with singular-value decomposition (Wise *et al.*, [1987]) has been used successfully to extract multiple relaxation-time constants from such traces.

Such studies have been carried out both for bulk GaAs and $Al_xGa_{1-x}As$/GaAs quantum-well structures. There are interesting differences in the relaxation dynamics of hot carriers in these cases (Taylor *et al.*, [1985]).

5.2. Femtosecond Relaxation Dynamics in Molecules

Ultrafast sources have also been used to study a variety of problems in molecular relaxation dynamics. One that is analogous to the semiconductor problem is the relaxation of excited vibronic states of dye molecules. As shown schematically in Fig. 10, the molecule is initially in the singlet ground electronic state S_0. A short pulse excites the molecule to an excited vibrational–rotational state of the singlet state S_1. The question is how long does the molecule stay in the initially excited state? This problem is analogous to the semiconductor problem discussed above. The same experimental arrangement can be used. The only difference is that the thin-film semiconductor sample is replaced by a thin dye jet of dilute solution of dye molecules dissolved in some solvent.

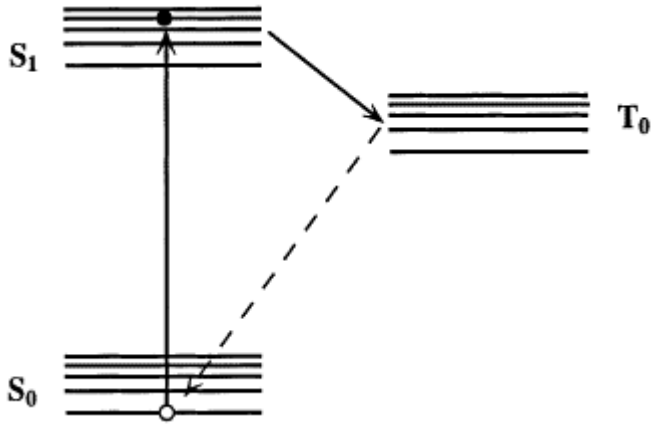

Figure 10 Schematic of $S_0 \rightarrow S_1$ excitation followed by $S_1 \rightarrow T_0$ relaxation transition in dye molecules.

The typical relaxation path of the molecules is that from the initially excited states the molecules relax to and thermalize near the bottom of the vibrational–rotational band of the S_1 state in much less than a picosecond and from there to the triplet state T_0 before eventually returning to the singlet ground states S_0 in a time on the order of microseconds to nanoseconds depending on the nature of the solvent. High–repetition-rate sources based on the mode-locked Rh6 G or Ti:sapphire laser at 10^8 Hz are ideal for studying the initial relaxation dynamics of such molecules in the femtosecond time domain. The general data analysis and experimental procedures are similar to those used for the semiconductor problems discussed above.

5.3. Coherent Wave-Packet Excitation and Relaxation in Molecules

In the case of molecules, in addition to the exponential relaxation processes, excitation and relaxation of coherent molecular vibrations in the form of quantum beats (Rosker *et al.*, [1986]) can also be observed using the femtosecond sources. An example of quantum beats observed (Wise *et al.*, [1987]) in optical-correlation spectroscopy is shown in Fig. 11 using the scheme shown in Fig. 6. The basic effect can be explained qualitatively (Tang, [1990]) in terms of the schematic diagram shown in Fig. 12. The first femtosecond pulse changes the electronic charge distribution in the molecule and excites the molecules from the ground electronic singlet state S_0 to the excited electronic singlet state S_1 with a corresponding change in the *equilibrium* configuration of the nuclear skeleton of the molecule. However, the heavier nuclei of the molecule do not have time to adjust to the new equilibrium configuration corresponding to the molecule in the excited electronic state during the first pulse. Because the molecule is left in a nonequilibrium configuration of the excited-state molecule at the end of the first pulse, it will oscillate around the equilibrium configuration in the excited state following excitation by the first pulse. This corresponds to excitation of a coherent vibrational wave packet in the S_1 state as shown schematically in Fig. 12. However, because of the Franck–Condon shift in the equilibrium configuration of the S_1 state from that of the ground state S_0, the excited coherent vibrational wave packet will oscillate around the new potential minimum. A delayed femtosecond pulse will sense this coherent wave-packet oscillation. This gives rise to the observed quantum beats in the transmission correlation trace. Damping in the coherent wave-packet oscillation gives the dephasing time of the corresponding vibrational states. Similar oscillations have now been seen in a great variety of molecules and in photodissociation kinetics.

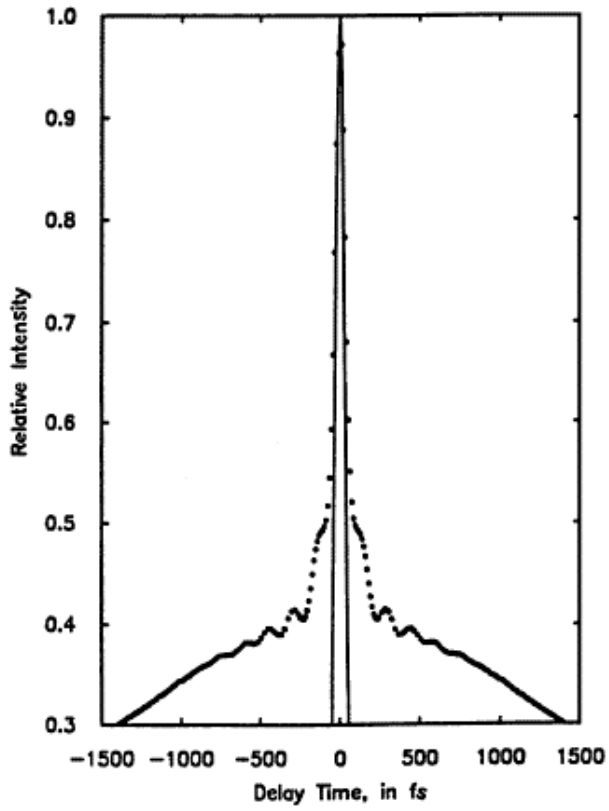

Figure 11 Example of transmission-correlation trace showing coherent wave-packet oscillation in the femtosecond time domain in malachite green.

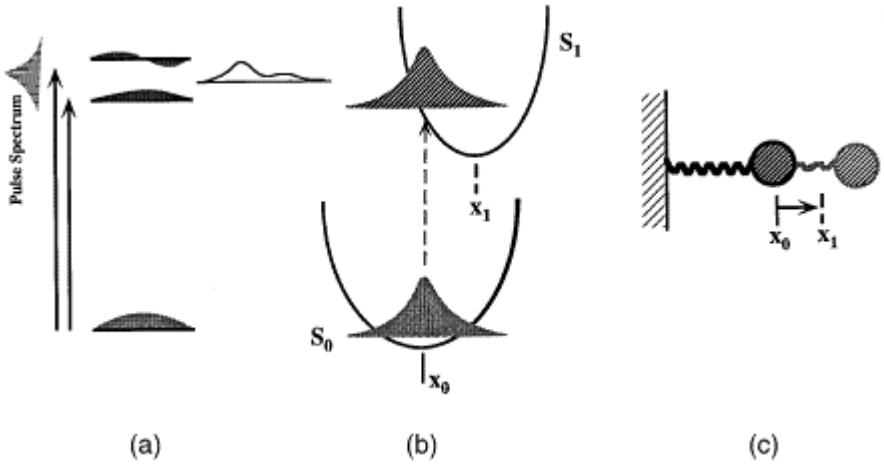

Figure 12 (a) Three-level model of coherent wave-packet excitation by an ultrashort pulse. (b) Schematic of excitation of vibrational wave packet in molecules. (c) Classical harmonic oscillator model of coherent wave-packet excitation in molecules. $S_{0,\ 1}$ = ground and first excited singlet states. $X_{0,\ 1}$ = equilibrium positions of $S_{0,\ 1}$ states.

The Zewail group at California Institute of Technology has developed and rigorously demonstrated a methodology by which ultrafast optical pulses can be used to explore chemical reactions (Zewail, [1994]). Typically, a femtosecond pulse initiates a reaction, and a subsequent probe pulse interrogates the transition state as it develops. Depending on the

nature of the potential-energy surface (PES) characterizing the reaction, a variety of dynamics are possible (Zewail, [1993], [1996]). In many cases, however, evolution along the PES will be oscillatory and will thereby lead to beat behavior. An excellent example is the dissociation of photoexcited alkali halides such as NaI, in which the probe pulse observes a resonance occurring along the reaction coordinate (Rose *et al.*, [1988]). These dynamics are attributable to the coherent oscillation of the excited-state wave packet in the potential well formed by the ionic/covalent avoided level crossing at 6.93-Å internuclear separation.

5.4. Coherent Wave-Packet Excitation and Relaxation in Coupled Quantum Wells

Analogous coherent electronic wave-packet excitation is also possible in coupled quantum wells. Consider a pair of coupled quantum wells with one of the layers selectively doped with deep donors as shown schematically in Fig. 13. If the barrier between the wells is such that the quantum-well states are coupled and the eigenstates of the coupled wells correspond to a symmetric and antisymmetric superposition of the individual quantum well states in analogy with the bonding and antibonding orbitals of a diatomic molecule, a suitable coherent superposition of the symmetric and antisymmetric coupled–quantum-well states leads to an electron wave packet confined in one or the other of the two wells. Such a coherent superposition state can be prepared by excitation, for example, from the deep donors selectively doped in one of the coupled quantum wells, as shown in Fig. 13. If the wavelength of the femtosecond pulse is tuned to correspond to the transition frequency from the donor to the coupled state and the bandwidth of the femtosecond pulse spans both the symmetric and antisymmetric states of the coupled quantum wells, the pulse can excite electrons from the donor level into the confined conduction-band states on the doped side of the coupled quantum wells initially. The excited electron wave packet will then oscillate between the two wells and can be observed with delayed probe pulses. Similar electron wave-packet oscillations from the confined valence-band states have already been observed by Leo *et al.* ([1991]).

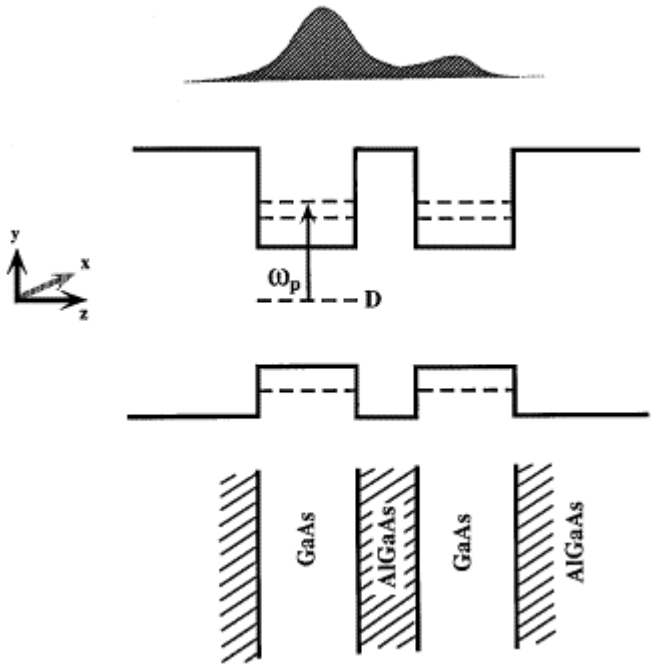

Figure 13 Coherent wave-packet excitation in modulation-doped coupled quantum wells.

Works Cited

- Agrawal G. P. (1989), *Nonlinear Fiber Optics*, New York: Academic Press.
- Baltuska A., Wei, Z., Pshenichnikov, M., Wiersma, D. (1997), *Opt. Lett.* **22**, 102–104.
- Boyd R. W. (1992), *Nonlinear Optics*, New York: Academic, pp. 275–281.
- Bullogh, R. K., Candney, P. J. (Eds.) (1980), *Solitons*, Heidelberg: Springer-Verlag.
- Chilla J. L. A., Martinez, O. E. (1993), *J. Opt. Soc. B* **10**, 638–643.
- deMaria A. J., Stetser, D. A., Heynau, H. (1966), *Appl. Phys. Lett.* **8**, 174–176.
- Doran N., Wood, D. (1988), *Opt. Lett.* **13**, 56–58.
- Duling I. N., III (1988), *Electron. Lett.* **24**, 1333–1334.
- Duling I. N., III (1991), *Electron. Lett.* **27**, 544–545.
- Dzhibladze M. I., Esiashvili, Z. G., Teplitskii, E. Sh., Isaev, S. K., Sagaradze, V. R. (1983) *Kvant. Elektron.* **10**, 432–434 [*Sov. J. Quantum Electron.* **13**, 245–247].
- Edelstein D. C., Wachman, E. S., Cheng, L. K., Bosenberg, W. R., Tang, C. L. (1988), *Appl. Phys. Lett.* **52**, 2211–2213.
- Edelstein D. C., Wachman, E. S., Tang, C. L. (1989), *Appl. Phys. Lett.* **54**, 1728–1730.
- Ellingson R. J., Tang, C. L. (1992), *Opt. Lett.* **17**, 343–345.
- Fork R. L., Green, B. I., Shank, C. V. (1981), *Appl. Phys. Lett.* **38**, 671–672.
- Fork R. L., Brito Cruz, C. H., Becker, P. C., Shank, C. V. (1987), *Opt. Lett.* **12**, 483–485.
- Geister G., Ulrich, R. (1988), *Opt. Commun.* **68**, 187–189.
- Goebel E. (1992), Ultrafast spectroscopy of semiconductors, *Opt. Photon. News* **3** (5), 33.
- Grudinin A. B., Richardson, D. J., Payne, D. N. (1992), Energy quantization in the figure eight fiber laser, *Electron. Lett.* **28**, 67–69.
- Haus H. A., Fujimoto, J. G., Ippen, E. (1991), *J. Opt. Soc. Am. B* **8**, 2068–2076.
- Haus H. A., Fujimoto, J. G., Ippen, E. (1992), *IEEE J. Quantum Electron.* **28**, 2086–2096.
- Hillegas C., Tull, J. X., Goswami, D., Strickland, D., Warren, W. S. (1994), *Opt. Lett.* **19**, 737–739.
- Hofer M., Fermann, M. E., Haberl, F., Townsend, J. E. (1990), *Opt. Lett.* **15**, 1467–1469.
- Hofer M., Ober, M. H., Haberl, F., Fermann, M. E. (1992), *IEEE J. Quantum Electron.* **JQE-28**, 720–728.

- Ippen E. P., Shank, C. V. (1977), Techniques for measurement in: S. L. Shapiro (Ed.), *Ultrashort Light Pulses*, New York: Springer-Verlag, pp. 87–92.
- Kafka J. D., Baer, T., Hall, D. W. (1989), *Opt. Lett.* **14**, 1269–1271.
- Kane D. J., Trebino, R. (1993), *J. Quantum Electron.* **29**, 571–579; *Opt. Lett.* **18**, 823–825 R.
- Krausz F., Fermann, M. E., Brabec, T., Curley, P. F., Hofer, M., Ober, M. H., Spielmann, C., Wintner, E., Schmidt, A. J. (1992), *IEEE J. Quantum Electron.* **QE-28**, 2097–2121.
- Leo K., Shah, J., Goebel, E., Damen, T. (1991), *Phys. Rev. Lett.* **66**, 201–204.
- Martinez O. E., Fork, R. L., Gordon, J. P. (1984), *Opt. Lett.* **9**, 156–158.
- New G. H. C. (1983), *Rept. Prog. Phys.* **46**, 877–971.
- Richardson D. J., Laming, R. I., Payne, D. N., Phillips, M. W., Matsas, V. J. (1991), *Electron. Lett.* **27**, 730–732.
- Rose T. S., Rosker, M. J., Zewail, A. H. (1988), *J. Chem. Phys.* **88**, 6672–6673.
- Rosker M. J., Wise, F. W., Tang, C. L. (1986), *Phys. Rev. Lett.* **57**, 321–324.
- Sala K. L., Kenny-Wallace, G. A., Hall, G. (1980), *IEEE J. Quantum Electron.* **QE-16**, 990–936.
- Salin F., Squier, J., Piche, M. (1991), *Opt. Lett.* **16**, 1674–1676.
- Shen Y. R. (1984), *Principles of Nonlinear Optics*, New York: Wiley Interscience, p. 518.
- Smith P. W., Duguay, M. A., Ippen, E. P. (1974), Mode Locking of Lasers in: J. H. Sanders, S. Stenholm (Eds.), *Progress in Quantum Electronics*, Vol. **3** Part 2, New York: Pergamon Press.
- Smith K., Greer, E. J., Wyatt, R., Wheatley, P., Doran, N. J., Lawrence, M. (1991), *Electron. Lett.* **27**, 244–245.
- Spence D. E., Kean, P. N., Sibbett, W. (1991), *Opt. Lett.* **16**, 42–44.
- Spence D. E., Sleat, W. E., Evans, J. M., Sibbett, W., Kafka, J. D. (1993), *Opt. Comm.* **101**, 286–296.
- Spence D. E., Wilandy, S., Tang, C. L., Bosshard, C., Gunter, P. (1996), *Appl. Phys. Lett.* **68**, 452–454.
- Spinelli, L., Couillaud, B., Goldblatt, N., Negus, D. K. (1991), Dig. CLEO '91, paper CPDP7, Washington, D.C.
- Stone J., Burrus, C. A. (1973), *Appl. Phys. Lett.* **23**, 388–390.
- Tamura K., Ippen, E. P., Haus, H. A., Nelson, L. E. (1993), *Opt. Lett.* **18**, 1080–1082.
- Tang C. L. (1990), Ultrashort Optical Pulses in: Lerner, G. L. Trigg (Eds.), *Encyclopedia of Physics*, 2nd ed., New York: VCH Inc., p. 1320.
- Tang C. L., Cheng, L. K. (1996), *Fundamentals of Optical Parametric Processes and Oscillators*, Chur, Switzerland: Harwood Academic Publishers.
- Tang C. L., Wise, F. W., Walmsley, I. A. (1988), *Rev. Mod. Opt.* **35**, 1939–1950.

- Taylor A. J., Erskine, D. J., Tang, C. L. (1985), *J. Opt. Soc. Am. B* **2**, 663–673.
- Trebino R., Kane, D. J. (1993), *J. Opt. Soc. Am. A*, **10**, 1101–1111.
- Weiner A. M. (1983), *IEEE J. Quantum Electron.* **QE-19**, 1276–1283.
- Weiner A. M., Leaird, D. E., Patel, J. S., Wullet, J. R. (1992), *IEEE J. Quantum Electron.* **28**, 908–919.
- Wise F. W., Rosker, M. J., Millhauser, G. L., Tang, C. L. (1987a), *J. Quantum Electron.* **QE-23**, 1116–1121.
- Wise F. W., Rosker, M. J., Tang, C. L. (1987b), *J. Chem. Phys.* **86**, 2827–2832.
- ZewailAhmed H. (1993), *J. Phys. Chem.* **97**, 12427–12446.
- Zewail A. H. (1994), *Femtochemistry—Ultrafast Dynamics of the Chemical Bond*, Singapore: World Scientific, Vols. **I** and **II**.
- ZewailAhmed H. (1996), *J. Phys. Chem.* **100**, 12701–12747.
- Zhang J., Huang, J. Y., Shen, Y. R. (1996), *Optical Parametric Generation and Amplification*, Chur, Switzerland: Harwood Academic Publishers.

- **Further Reading** The proceedings of the continuing bi-annual Ultrafast Phenomena Conferences published by Springer-Verlag are a good source of information.

GLOSSARY

Chirping in a Pulse: A change in carrier frequency of a pulse within the pulse duration.

Coherence Properties: Temporal and spatial properties related to the phase of a wave.

Coherent Wave Packet: A molecular state corresponding to a coherent superposition of several eigenstates of the molecule. In the spatial domain, such a coherent superposition of wave functions forms a wave packet.

Convolution and Deconvolution: Convolution of two functions means the integral of the product with one of the functions and the other with a fixed delay. Deconvolution is the inverse process by which one of these functions is obtained from the convolution of the two and the other function.

External-Cavity Semiconductor Lasers: Semiconductor lasers whose cavity is formed by external mirrors rather than the cleaved facets of the semiconductor crystal.

Extraordinary and Ordinary Waves: Waves whose electric field is, respectively, in the plane or perpendicular to the plane defined by the optical axis of the medium and the propagation vector of the wave.

Franck–Condon Shift: Shift in the minima of the potential curves corresponding to different electronic states of a molecule in the configuration-coordinate space.

Group-Velocity Dispersion: Difference in group velocities at different frequencies or

wavelengths.

Heavy and Light Holes: Valence-band states of semiconductors whose equivalent hole masses are considered heavy or light.

Isomorphs: Crystals of similar structures with analogous ionic groups.

Longitudinal Modes: Laser oscillation modes with different spatial variations along the axis of the laser cavity.

Mode Locking: Lasers tend to oscillate in many modes of the optical cavity. The frequencies of these modes are approximately equally spaced, and the phases of these modes are generally not related to each other. Mode locking refers to any arrangement by which the modes are forced to be precisely equally spaced and to have exactly the same phase.

Parametric Conversion: Conversion of light wave from one wavelength to other longer wavelengths by nonlinear optical processes.

Quantum Beat: Beating due to interference in the time domain of different eigen-functions of a quantum-mechanical system.

Quantum Well: Potential wells on a dimensional scale small enough so that quantum effects become important.

Relaxation Dynamics: The dynamics corresponding to the return to equilibrium of a perturbed system.

Saturable Absorber: An absorber whose absorption changes nonlinearly with increasing intensity and eventually levels off to a constant value at high intensity.

Second-Order Autocorrelation Function: Time-averaged product of a signal and the same signal with a fixed delay as a function of the delay. Equation (15) is an example of second-order intensity autocorrelation of a light wave.

Self-Phase Modulation: In an optical medium with light-induced intensity-dependent index of refraction, the phase of the light wave can thus be modulated by the light wave itself.

Soliton: A pulse of a special form such that the dispersion effect cancels exactly the self-phase-modulation effect in the medium and the shape of the pulse remains the same upon propagation.

Transform-Limited Pulse: A pulse with an envelope whose shape corresponds to the Fourier transform of its spectrum.

Vibronic State: Vibrational state of a given electronic state of a molecule.